Advances in the Theory of Nonlinear Analysis and its Applications 7 (2023) No. 1, 61–81.
https://doi.org/10.31197/atnaa.1187342
Available online at www.atnaa.org
Research Article

Advances in the Theory of Nonlinear Analysis and its Applications

ISSN: 2587-2648

Peer-Reviewed Scientific Journal

Heat transfer analysis of Radiative-Marangoni Convective flow in nanofluid comprising Lorentz forces and porosity effects

Islam Zari[a], Taza Gul[b], Karlygash Dosmagulova[c], Tahir Saeed Khan[d], Safia Haq[e]

[a]*University of Peshawar, Khybar Pakhtunkhwa, Pakistan*

[b]*Department of Mathematics, City University of Science and Information Technology, Peshawar, Khybar Pakhtunkhwa, Pakistan. Engineering Department, Cambridge Graphene Centre, Electrical Engineering Division, Cambridge University, Cambridge, United Kingdom.*

[c]*Department of Mathematics, Al-Farabi Kazakh National University, Almaty, Kazakhstan. Department of Mathematics: Analysis Logic and Discrete Mathematics, Ghent University, Ghent, Belgium*

[d]*Department of Mathematics, University of Peshawar, Khybar Pakhtunkhwa, Pakistan.*

[e]*Jinnah College for Women, University of Peshawar, Khybar Pakhtunkhwa, Pakistan.*

Abstract

The present work investigates the impacts of the Lorentz forces, porosity factor, viscous dissipation and radiation in thermo-Marangoni convective flow of a nanofluids (comprising two distinct kinds of carbon nanotubes (CNT_s)), in water (H_2O). Heat transportation developed by Marangoni forces happens regularly in microgravity situations, heat pipes, and in crystal growth. Therefore, Marangoni convection is considered in the flow model. A nonlinear system is constructed utilizing these assumptions which further converted to ordinary differential equations (ODEs) by accurate similarity transformations. The homotopic scheme is utilized to compute the exact solution for the proposed system. The study reveals that higher estimations of Hartmann number and Marangoni parameter speed up the fluid velocity while the opposite behavior is noted for porosity factor. Further, the rate of heat transfer shows upward trend for the Hartmann number, Marangoni parameter, nanoparticle solid volume fraction, radiation parameter whereas a downward trend is

Email addresses: zarimaths@uop.edu.pk (Islam Zari), tazagul@cusit.edu.pk (Taza Gul), karlygash.dosmagulova@ugent.be (Karlygash Dosmagulova), tsk7@uop.edu.pk (Tahir Saeed Khan), safiahaq@uop.edu.pk (Safia Haq)

Received July 30, 2022; Accepted: November 7, 2022; Online: November 24, 2022.

followed by the Brinkman number and porosity factor. It is fascinating to take observe that contemporary analytical outcomes validate the superb convergence with previous investigation.

Keywords: Marangoni boundary layer flow $SWCNT_s/MWCNT_s$ Lorentz forces Viscous dissipation Porosity effect.
2010 MSC: 80A20,80A23,80A97.

Nomenclature:

A	positive dimensionless constant
B_r	Brinkmann number
b_0	width of magnets and electrode
c_p	heat specific capacity
j_0	applied current density of electrodes
$k*$	mean absorption coefficient
L	length of surface
M_0	magnetization of the permanent magnets
M	Marangoni parameter
$Nu_{\hat{x}}$	local Nusstle number
n_e	exponent constant
Pr	Prandtl number
Q_h	Hartmann number
q	dimensionless quantity
R_s	Radiation parameter
T	Temperature of nanofluid
T_w	Temperature of fluid at Riga plate
T_∞	nanofluidic temperature far away from the Riga surface
Greek symbols	
α_{nf}	nanofluid effective density
γ_T	coefficient of temperature by surface tension
g	dimensionless temperature
$\sigma*$	Stefen Boltzman constant
η	similarity variable
ρ_{nf}	nanofluid density
k_{nf}	thermal conductivity of nanofluid
λ_p	porosity factor
ν	kinematic viscosity
σ_T	temperature gradient of surface tension
δ	surface tension
δ_0	constant
ΔT	constant characteristic temperature
ϕ_n	volume of solid fraction
ψ	stream function

1. Introduction

An increased rate of heat transfer in numerous devices with high speed flow is one of the major issues of present-day innovation. Therefore, it is essential to ensure adequate cooling system due to its applications in industry [1-2]. This problem can be solved by making use of nanofluids. The classical fluids' thermal conductivity can be enhanced by nanofluids in fluid systems. [3] were the first analyst who introduced the revolutionary idea of nanofluids comprising a base fluid with suspended nanoparticles. [4] highlighted the heat transportation process in nanoparticles of radiative heat flux in nanomaterials. He analyzed that suspension of the nanoparticles enhances the temperature and decreases the surface heat flux. Rana et al. [5] studied the nanofluidic flow moving through a vertical plate and discussed the different impacts of nanoparticle by the use of revised model of Buongiorno. They noticed that the nanoparticles aggregation drastically intensified the temperature whereas the velocity become decreased. Swain and Mahanthesh [6] observed the increasing behavior of magneto based three-dimensional radiating nanoliquid with different effects. Results suggest that the nanoparticles aggregation substantially enhances the thermal property and impact of magnetism is greater in ordinary fluid flow in comparison to classical nanoliquid. Mahanthesh et al. [7] numerically solved the MHD flow of nanoliquid past a bidirectional stretching plate. Sabu et al. [8] explored the kinematics aggregation of nanoparticle on MHD- convective flow of nanomaterial over a flat surface with sensitivity evaluation. Results show that the fluid motion significantly decreases as the plate's inclination increases, while temperature is improved. Ahmed et al. [9] performed a numerical study of the hydraulic driven thermal execution of nanofluids in a scraped channel stream utilizing hybrid nanoparticles. Results witnessed that the high amount of nanoparticles's volume fraction, the rate of heat transfer and pressing factor adopted an upward trend. In center of a square based chamber, an impact of volume fraction and radiation on (CNT_s) nanoliquid stream is inquired by Reddy et al. [10]. They investigated that the 5 percent amount of $SWCNT_s$ is added to base fluid, expanded up to 6 percent the nanofluid heat transfer rate. Also, numerous investigations relevant to the nanofluids have been done in [11-15].

Interfacial phenomena are one of incredible areas of heat transfer processes. The interfacial boundary (the boundary between two phases), has very distinct characteristics compared to the bulk phase and has importance in a variety of chemical engineering procedures. The interface between two phases may control the transportation process, for instance, the reaction at the interface, adsorption, heterogeneous catalysis, and liquid-liquid extraction. One of the sophisticated techniques which focuses on the interface between different phases is Marangoni (thermo-capillary) convection. The Marangoni convection implies the mass exchange because of gradients of the surface tension among fluids (gas-gas or gas-liquid) interfaces. In 1855, this fascinating idea is initially presented by James Thomson a physicist as "tears of wine". There is numerous viable utilization of Marangoni convection like adjustment of cleanser films, utilized in the manufacturing of an incorporated circuit, Benard cell or convection cell and to dry the silicon wafer [16-19]. Gul et al. [20] worked on the MHD based film stream of lamp oil contains nanofluid affected by Marangoni convection. They observed the upward trend in a fluid motion for the larger amount of the Marangoni number. Zhang et al. [21] investigated heat and flow transference in a Maxwell fluid flow in the presence of Marangoni convection. They noticed that enhancing the Marangoni convection brings a decline in the film thickness. Gul et al. [22] studied the Marangoni convective flow based on Graphyne Oxide nanofluids by integer and non-integer orders. Qayyum et al. [23] elucidated the dynamical hybrid nanofluid related fluid flow with existence of Marangoni convection. The study reveals that high performance is found in heat transfer rate for a larger amount of Marangoni number.

The behavior of electrically controlled fluids for instance, plasma, fluid metals, and electrolytes can be controlled and altered by introducing magnetic fields in the flow. This kind of flow, traditionally called as electro-magnetohydrodynamic (EMHD), assumes an important part in field of science and modern approaches, for instance, in designing, astronomy quakes, and sensors. However, in some EMHD flows, where the magnetic field does not induce strong currents in the flow, the external electric powers are applied. For this purpose, a researcher named Gailitis [24] introduced the power agent known as Riga plate which put together the magnetic/electric fields at the same time and, accordingly, which can make a divider corresponding to the Lorentz forces in leading liquids. Vaidya et al. [25] looked into the effect of nanofluid flow with mixed convection past a stretching Riga surface. Results show that For better amount of Hartmann number, the fluid speed enhances and temperature suppresses. Khashi'ie et al. [26] explored the phenomenon of the stagnation point flow with suction property of hybrid nanofluid over a Riga plate. They determined that the temperature was increased for the larger amount of EMHD parameter, mixed convection, and suction parameter. Nazeer et al. [27] addressed the scale analysis numerically for the Powell based Eyring nanofluid over a stretching Riga plate in the presence of an internal resistance and entropy generation. They imple-

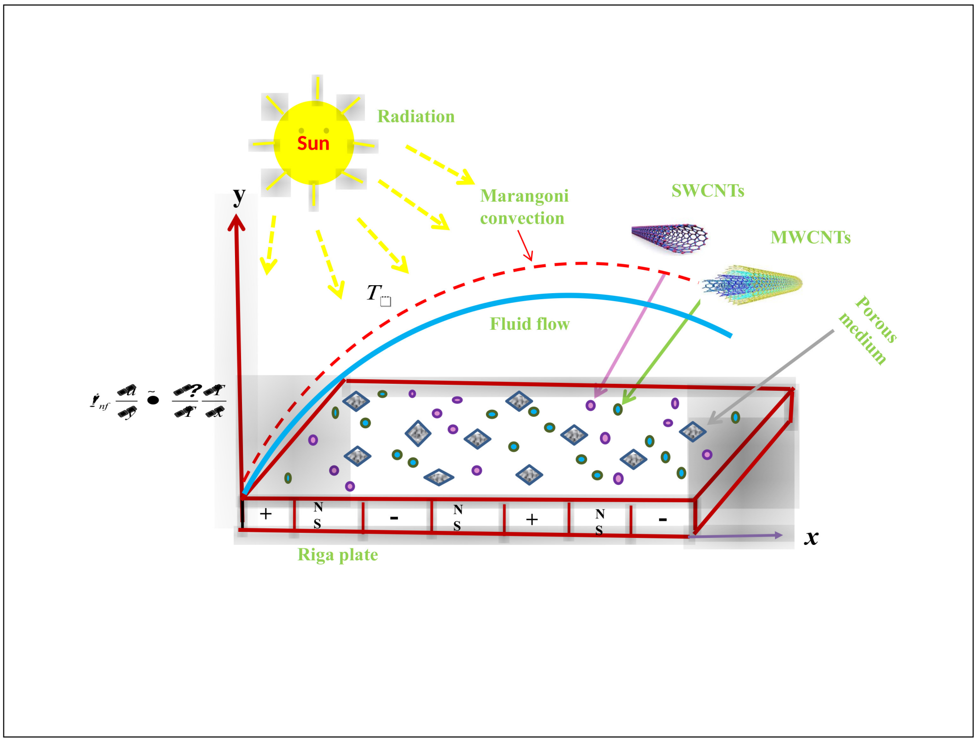

Figure 1: Flow configuration.

mented the Shooting method for accurate results and fast convergence. Bhatti and Michaelides [28] worked on Riga plate of Arrhenius activated energy with thermo-bio-convective nanofluid. It is observed from the consequences that the bio-convection Rayleigh number and magnetic field weaken the velocity profile. Iqbal et al. [29] addressed the heat transfer with melting phenomenon with erratic thickness of the nanofluidic model towards a Riga plate. They employed the Keller Box scheme to simulate the highly nonlinear problem. Also, some other relevant fantastic studies can be seen in the literature [30-34].

In heat flux related problems, the influences of different types of nanofluids have been studied with distinct systematic approaches by the researchers. However, To the quality of the authors expertise, no enterpriser has yet been indorsed to use the Marangoni convection over a porous Riga plate. Mostly, the researchers give preference to deal with flow field through moving surfaces, while the novelty of present research is to observe the effects of Lorentz forces generated by Riga plate and porosity phenomena in Marangoni convection. Hence, a new model of two types of nanoliquid (i.e., Water- $SWCNT_s$ and Water- $MWCNT_s$) because of Marangoni convective flow on a porous Riga surface when solar radiation and viscous dissipative phenomena are constructed and simulated through homotopy analysis method (HAM) in literature [35-40] to achieve the above-highlighted flow characteristics. Additionally, the validity of HAM solution is crystal clear in comparison to Galerkin Finite Element Method (GFEM) for concerned liquid parameters.

2. Flow model

A steady, incompressible 2D, Marangoni (thermo-capillary) convection of nanofluids ($CNT_s - H_2O$) on a Riga plate is taken into account. A Marangoni boundary constraint is considered as for this proposed model. $(\widehat{x}, \widehat{y})$ is a system of cartesian coordinate $(\widehat{x}, \widehat{y})$ is considered, where flow direction towards $\widehat{x}-$ axis and perpendicular direction of flow is taken by $\widehat{y}-$ axis. Two fluids are immiscible at an interface and the thermal layer thickness decreases because of Riga plate therefore, free surface is assumed to be flat. $\widehat{T}_w = \widehat{T}_\infty + A\widehat{x}^{n_e+1}$ is considered as the temperature variable on the interface, where the outer flow temperature is $\widehat{T}_\infty$. Heat transfer rate is studied with the film subjected to dissipated viscous film and thermal radiative phenomena. The porosity impact on the fluid flow are also part of the proposed model and its physical structure can be evoked in Figure 1. Under all assumptions, the mathematical structure of present flow can be written as

Conservation of Mass [40-43]

$$\frac{\partial \widehat{v}}{\partial \widehat{y}} = -\frac{\partial \widehat{u}}{\partial \widehat{x}}, \tag{1}$$

Conservation of Linear Momentum [40], [43]

$$\widehat{u}\frac{\partial \widehat{u}}{\partial \widehat{x}} = -\widehat{v}\frac{\partial \widehat{u}}{\partial \widehat{y}} + \frac{\mu_{nf}}{\rho_{nf}}\frac{\partial^2 \widehat{u}}{\partial \widehat{y}^2} - \frac{\mu_{nf}}{\rho_{nf}}\frac{\widehat{u}}{\tilde{k_0}} + \frac{\pi M_0 j_0 Exp[\frac{-\pi}{b_0}\widehat{y}]}{8\rho_{nf}}, \tag{2}$$

Conservation of Energy [40-41]

$$\widehat{u}\frac{\partial \widehat{T}}{\partial \widehat{x}} = -\widehat{v}\frac{\partial \widehat{T}}{\partial \widehat{y}} + \frac{\mu_{nf}}{(\rho c_p)_{nf}}(\frac{\partial \widehat{u}}{\partial \widehat{y}})^2 + \frac{k_{nf}}{(\rho c_p)_{nf}}\frac{\partial^2 \widehat{T}}{\partial \widehat{y}^2} - \frac{1}{(\rho c_p)_{nf}}\frac{16\sigma^* \widehat{T}_\infty^3}{3k^*}\frac{\partial^2 \widehat{T}}{\partial \widehat{y}^2}, \tag{3}$$

Boundary conditions [40-43]

$$\begin{aligned} \frac{\partial \widehat{u}}{\partial \widehat{y}} = -\frac{1}{\mu_{nf}}\frac{\partial \widehat{T}}{\partial \widehat{x}}\frac{d\delta}{d\widehat{T}}, \quad \widehat{T}_\infty, \quad \widehat{u} \to \infty, \quad \text{at} \quad \widehat{y} \to \infty, \widehat{v} = 0, \\ \widehat{T} = \widehat{T}_w \quad \text{at} \quad \widehat{y} \to 0, \end{aligned} \tag{4}$$

Here, the cartesian velocity coordinates are $(\widehat{u}, \widehat{v})$ in directions of $\widehat{x}$ and $\widehat{y}$, μ_{nf} is the nanofluid dynamical viscosity, ρ_{nf} is the nanofluid density, $\tilde{k}$ is porosity parameter, j_0 is the density of applied current inside the electrodes, M_0 is the permanent magnetization, b_0 is the electrode and magnets width, k_{nf} is thermo-conductivity , $(c_p)_{nf}$ is heat capacity, σ^* is Boltzman Stefan constant, and k^* is absorption mean coefficient, $\widehat{T}$ is fluid temperature, $\widehat{T}_\infty$ is an external flow temperature, $\widehat{T}_w$ is wall temperature, δ is the surface tension and $\delta = (\widehat{T} - \widehat{T}_\infty)\frac{\gamma_{\widehat{T}}}{2} + \delta_0$ where, δ_0 is constant with positive values, $\gamma_{\widehat{T}} = -\frac{\partial \delta}{\partial \widehat{T}}|_{\widehat{T}=\widehat{T}_\infty}$ and $\mu_{nf}\frac{\partial \widehat{u}}{\partial \widehat{y}} = -\frac{d\delta}{d\widehat{T}}\frac{\partial \widehat{T}}{\partial \widehat{x}}$ denotes Marangoni condition at the interface.

ψ is the stream function where $\widehat{u} = \frac{\partial \psi}{\partial y}$ and $\widehat{v} = -\frac{\partial \psi}{\partial x}$ is presented in Equations (1)-(4) to achieve

$$\begin{aligned} -\frac{\partial \psi}{\partial x}\frac{\partial^2 \psi}{\partial y^2} = &- \frac{\partial \psi}{\partial y}\frac{\partial^2 \psi}{\partial x \partial y} + \frac{\mu_{nf}}{\rho_{nf}}\frac{\partial^3 \psi}{\partial y^3} - \\ &- \frac{\mu_{nf}}{\rho_{nf} k_0}\frac{\partial \psi}{\partial y} + \frac{\pi M_0 j_0 e^{[\frac{-\pi.\eta}{b_0 \widehat{x}^{\frac{n_e-1}{3}} (\frac{\sigma_{\widehat{T}} \Delta T \rho_f}{L^{n_e+1}\mu_f^2})^{\frac{1}{3}}}]}}{8\rho_{nf}}, \end{aligned} \tag{5}$$

$$\begin{aligned} \frac{\partial \psi}{\partial y}\frac{\partial \widehat{T}}{\partial \widehat{x}} = &\frac{\partial \psi}{\partial x}\frac{\partial \widehat{T}}{\partial \widehat{y}} + \frac{\mu_{nf}}{(\rho c_p)_{nf}}(\frac{\partial^2 \psi}{\partial \widehat{y}^2})^2 + \\ &+ \frac{k_{nf}}{(\rho c_p)_{nf}}\frac{\partial^2 \widehat{T}}{\partial \widehat{y}^2} - \frac{1}{(\rho c_p)_{nf}}\frac{16\sigma^* \widehat{T}_\infty^3}{3k^*}\frac{\partial^2 \widehat{T}}{\partial \widehat{y}^2}, \end{aligned} \tag{6}$$

$$\begin{aligned}\mu_{nf}\frac{\partial^2\psi}{\partial\widehat{y}^2} = -\frac{d((\widehat{T}-\widehat{T}_\infty)\frac{\gamma_{\widehat{T}}}{2}+\delta_0)}{d\widehat{T}}\frac{\partial\widehat{T}}{\partial\widehat{x}}, \quad \frac{\partial\psi}{\partial x} = 0,\\ \widehat{T} = \widehat{T}_w \quad \text{at} \quad \widehat{y}\to 0,\\ \widehat{T}\to\widehat{T}_\infty, \quad \frac{\partial\psi}{\partial y}\to\infty, \quad \text{at} \quad \widehat{y}\to\infty.\end{aligned} \tag{7}$$

Here, $\mu_{nf}\frac{\partial^2\psi}{\partial\widehat{y}^2} = -\frac{d((\widehat{T}-\widehat{T}_\infty)\frac{\gamma_{\widehat{T}}}{2}+\delta_0)}{d\widehat{T}}\frac{\partial\widehat{T}}{\partial\widehat{x}}$ shows the Marangoni term.

The main difference among natural and thermocapillary (Marangoni flow) convection is that in natural convection, the fluid motion is encouraged by natural way while, in thermocapillary convection, the fluids motion is encouraged by temperature-induced surface tension gradients means [42-49].

Nanofluid properties [20], [43], [50]

$$\begin{aligned}(1-\phi_n)^{2.5}\mu_{nf} = \mu_f,\\ \breve{k}_{nf} = ln\frac{\breve{k}_{CNT}+\breve{k}_f}{2\breve{k}_f}.\breve{k}_f\frac{2\phi_n\frac{\breve{k}_{CNT}}{\breve{k}_{CNT}-\breve{k}_f}+(1-\phi_n)}{2\phi_n ln\frac{\breve{k}_{CNT}+\breve{k}_f}{2\breve{k}_f}}.\frac{\breve{k}_f}{\breve{k}_{CNT}-\breve{k}_f}+(1-\phi_n),\\ (\rho c_p)_{nf} = (\rho c_p)_f(1-\phi_n)+\phi_n(\rho c_p)_{CNT}.\end{aligned} \tag{8}$$

Similarity transformations [40], [51]

$$\begin{aligned}\psi(\widehat{x},\widehat{y}) = \widehat{x}^{\frac{n_e+2}{3}}f(\eta)(\frac{\sigma_{\widehat{T}}\Delta\widehat{T}\mu_f}{L^{n_e+1}\rho_f^2})^{\frac{1}{3}}, \quad \eta = \widehat{x}^{\frac{n_e-1}{3}}\widehat{y}(\frac{\sigma_{\widehat{T}}\Delta\widehat{T}\rho_f}{L^{n_e+1}\mu_f^2})^{\frac{1}{3}},\\ \widehat{T}_w = \frac{\Delta\widehat{T}}{L^{n_e+1}}\widehat{x}^{n_e+1}g(\eta)+\widehat{T}_\infty.\end{aligned} \tag{9}$$

Here, ψ is known as stream function, $\sigma_{\widehat{T}}$ is for surface tension, $\Delta\widehat{T}$ is temperature characteristic, L is surface length, respectively.

Transformed system of ODEs

$$\begin{aligned}(1-\phi_n)^{-2.5}f''' + (\frac{\rho_{CNT}}{\rho_f}\phi+1+\phi)[\frac{n_e+2}{3}ff'' - \frac{2n_e+1}{3}f'^2]-\\ -(1-\phi_n)^{-2.5}M\lambda_p f' + Q_h e^{[-q\eta]} = 0,\end{aligned} \tag{10}$$

$$\begin{aligned}(\frac{k_{nf}}{k_f}+R_n)g'' - [\frac{(\rho c_p)_{CNT}}{(\rho c_p)_f}\phi_n+1-\phi_n](n_e+1)gf'+\\ [(\rho c_p)_{CNT}((\rho c_p))_f^{-1}\phi_n+1-\phi_n]P_r(n_e+2)3^{-1}fg'\\ +(g'')^2.(1-\phi_n)^{-2.5}B_r,\end{aligned} \tag{11}$$

$$\begin{aligned}f = 0, \quad f'' = -(1-\phi_n)^{2.5}(1+n_e), \quad g = 1, \text{at} \quad \eta = 0,\\ f'\to 0, \quad g\to 0, \quad \eta\to\infty.\end{aligned} \tag{12}$$

Here, λ_p is the porosity factor, M is Marangoni number, R_s is radiation, P_r is well-known Prandtl parameter, B_r is Brinkmann parameter, Q_h is Hartmann number, and q is the dimensionless positive constant,

Table 1: Thermal physical values for selected nanoparticles and proposed base fluid Shafiq et al. [43]

Physical characteristics	H_2O	$SWCNT_s$	$MWCNT_s$
$\breve{\rho}(kg/m^3)$	$\frac{9971}{10}$	2600.0	1600.0
$\breve{c}_p(J/kgK)$	04179	425.0	796.0
$\breve{k}(W/mK)$	$\frac{613}{1000}$	6600.0	3000.0

respectively. Mathematically, the variables are

$$\lambda_p = \frac{\mu_f^{\frac{4}{3}}}{k_0}, \quad M = \frac{L^{\frac{2n_e+2}{3}}}{\sigma_T^{\frac{2}{3}} \Delta T^{\frac{2}{3}} \rho_f^{\frac{2}{3}}}, \quad R_s = \frac{4\sigma * T_\infty^3}{k_f k*},$$
$$P_r = \frac{\nu_f}{\alpha_f}, B_r = \frac{\sigma_T \Delta T \mu_f^{-12\frac{4}{3}}}{k_f L^{\frac{(n_e+1)}{3}}} \widehat{x}^{\frac{-1+n_e}{3}}, \tag{13}$$
$$Q_h = \frac{\mu_f^{\frac{2}{3}} L^{\frac{(n_e+1)}{3}} \pi M_0 J_0}{8\sigma_T^{\frac{4}{3}} \Delta T^{\frac{1}{3}}}, \quad q = \frac{\pi}{b_0} (\frac{L^{n+1} \mu_f^2}{\sigma_T \Delta T \rho f})^{\frac{1}{3}}.$$

Further, the thermal physical characteristics of H_2O/CNT_s are presented in Table 1.

In a fluid, the ratio between convection to conduction at a boundary is the Nusselt number. Convection comprises both diffusion and advection. The physical coverage of engineering interest is Nusselt value, which is stated as Chaudhary et al. [40].

$$Nu_{\widehat{x}} = -(R_s + B)(\frac{\sigma_T \Delta T \rho_f}{L^{n_e+1} \mu_f^2})^{\frac{1}{3}} \widehat{x}^{\frac{n_e+2}{3}} g^{'}(0). \tag{14}$$

Here, $R_s = \frac{4\sigma * T_\infty^3}{k_f k*}$ is for radiation and $B = \frac{k_{nf}}{k_f}$ is ratio between the nanofluid and base fluid's thermal conductivity.

3. Analytical solution

The homotopy analysis method is selected to obtain the series solution of underlying model [44-45]. This procedure starts by considering initial base functions, which can be written as Noeiaghdam et al. [46].

$$\widehat{f_0}(\eta) = (1 - exp(-\eta))(1 + n_e)(1 - \phi_n)^{2.5}, \quad \widehat{g_0}(\eta) = exp(-\eta), \tag{15}$$

the solution cannot exist properly without the following nonlinear operators by Chen et al. [47].

$$L_{\widehat{f}}(\widehat{f}) = -\frac{d\widehat{f}}{d\eta} + \frac{d^3\widehat{f}}{d\eta^3}, \quad L_{\widehat{g}}(\widehat{g}) = -\widehat{g} + \frac{d^2\widehat{g}}{d\eta^2}, \tag{16}$$

along with (Chen et al. [47])

$$L_{\widehat{f}}[M_1 + J_2 e^{\eta} + M_3 e^{-\eta}] = 0, \qquad L_{\widehat{g}}[M_4 e^{\eta} + M_5 e^{-\eta}] = 0. \tag{17}$$

Here, M_i are arbitrary values, where $i = 1-5$. The zero order problem can be presented in the following way

$$L_{\widehat{f}}[\widehat{f}-\widehat{f}_0].(1-p) = p\hbar_{\widehat{f}}\mathcal{L}_{\widehat{f}}\left[\widehat{f}\right], \tag{18}$$

$$\left.\frac{\partial\widehat{f}}{\partial\eta}\right|_{\eta\,=\,0} = 0, \quad \left.\frac{\partial^2\widehat{f}}{\partial\eta^2}\right|_{\eta\,=0} = -\frac{(1+n_e)}{(1-\phi_n)^{2.5}}, \quad \left.\frac{\partial\widehat{f}}{\partial\eta}\right|_{\eta\,\to\infty} = 0, \tag{19}$$

$$L_{\widehat{g}}[\widehat{g}.(1-p)-\widehat{g}_0] = p\hbar_{\widehat{g}}\mathcal{L}_{\widehat{g}}\left[\widehat{g},\widehat{f}\right], \tag{20}$$

$$\widehat{g}|_{\eta\,=\,0} = 1, \qquad \widehat{g}|_{\eta\to\infty} = 0. \tag{21}$$

The operators which are nonlinear can be stated as

$$\begin{aligned}\mathcal{L}_{\widehat{f}}(\widehat{f}) = (1-\phi_n)^{-2.5}\widehat{f}''' + (1+\frac{\rho_{CNT}}{\rho_{\widehat{f}}}\phi_n)(\frac{n_e+2}{3})\widehat{f}\widehat{f}'' - \\ (1+\frac{\rho_{CNT}}{\rho_{\widehat{f}}}\phi_n+\phi_n)(\frac{2n_e+1}{3})\widehat{f}'^2 \\ -(1-\phi_n)^{-2.5}\lambda_p M\widehat{f}' + Q_h e^{-q\eta},\end{aligned} \tag{22}$$

$$\begin{aligned}\mathcal{L}_{\widehat{g}}(\widehat{f},\widehat{g}) = \widehat{g}''(R_s + k_{nf}(k_f)^{-1}) + \\ +((\rho c_p)_{CNT}((\rho c_p)_{\widehat{f}})^{-1}\phi_n + 1 - \phi_n)P_r(\frac{n_e+2}{3})\widehat{f}\widehat{g}' \\ -(\frac{(\rho c_p)_{CNT}}{(\rho c_p)_{\widehat{f}}}\phi_n + 1 - \phi_n)\widehat{g}'(n_e+1)\widehat{f}' + B_r(\widehat{g}'')^2(1-\phi_n)^{-2.5}\end{aligned} \tag{23}$$

Here, $0 \le p \le 1$ and $\hbar_{\widehat{f}}$ and $\hbar_{\widehat{g}}$ are auxiliary values which are zero free.

The mth order model is

$$L_{\widehat{f}}[\widehat{f}_m - \chi_m\widehat{f}] = \hbar_{\widehat{f}}N_m^{\widehat{f}}, \tag{24}$$

$$\frac{\partial\widehat{f}_m}{\partial\eta}|_{\eta\to\infty} = 0, \;\; \widehat{f}_m|_{\eta=0} = 0 \;\; \frac{\partial^2\widehat{f}_m}{\partial\eta^2}|_{\eta=0} = 0, \tag{25}$$

$$L_{\widehat{g}}[\widehat{g}_m - \chi_m\widehat{g}_{m-1}] = \hbar_{\widehat{g}}N_m^{\widehat{g}}, \tag{26}$$

$$\widehat{g}|_{\eta\to\infty} = 0 \quad ,\widehat{g}|_{\eta=0} = 0, \tag{27}$$

$$\begin{aligned} N_m^{\widehat{f}} &= (1-\phi_n)^{-2.5}\widehat{f}_{m-1}^{'''}+ \\ &+(\frac{\rho_{CNT}}{\rho_{\widehat{f}}}\phi_n+1+\phi_n)(\frac{n_e+2}{3})\sum_{k=0}^{m-1}\widehat{f}_k\widehat{f}_{m-1-k}^{'}- \\ &-(\frac{\rho_{CNT}}{\rho_{\widehat{f}}}\phi_n+1+\phi_n)(\frac{2n_e+1}{3})\sum_{k=0}^{m-1}\widehat{f}_k^{''2}- \\ &-(1-\phi_n)^{-2.5}M\lambda_p\sum_{k=0}^{m-1}\widehat{f}_k^{'}+Q_h exp[-q\eta], \end{aligned} \tag{28}$$

$$\begin{aligned} N_m^{\widehat{g}} &= (\frac{k_{nf}}{k_f}+R_s)\widehat{g}_{m-1}^{''}+ \\ &+(\frac{(\rho c_p)_{CNT}}{(\rho c_p)_{\widehat{g}}}\phi_n+1-\phi_n)P_r(\frac{n_e+2}{3})\widehat{f}_{m-1-k}\widehat{g}_k^{'}- \\ &-[((\rho c_p)_{\widehat{f}})^{-1}(\rho c_p)_{CNT}\phi_n+1- \\ &-\phi_n](n_e+1)\widehat{g}_{m-1-k}\sum_{k=0}^{m-1}[r\widehat{f}_k^{'}+(1-\phi_n)^{-2.5}\sum_{k=0}^{m-1}B_r\widehat{g}_{k^2}^{''}, \end{aligned} \tag{29}$$

where

$$\chi_{\hat{m}} = \begin{cases} 0.0 & \text{if } \hat{m} \le 1, \\ 1.0 & \text{if } \hat{m} > 1. \end{cases} \tag{30}$$

For $p = 0.0$,

$$\widehat{f} = \widehat{f}_0, \qquad \widehat{g} = \widehat{g}_0, \tag{31}$$

For $p = 1.0$,

$$\widehat{f} = f, \qquad \widehat{g} = \widehat{g}. \tag{32}$$

$\widehat{f}$ and $\widehat{g}$ are the problem solutions which is change from the initial solutions $\widehat{f}_0$ and $\widehat{g}_0(\eta)$ to terminal solutions $\widehat{f}$ and $\widehat{g}$, respectively. In addition, Taylor's series is:

$$\widehat{f} = \sum_{m=1}^{\infty}\widehat{f}_m p^m + \widehat{f}_0, \;\; \widehat{f}_m = (m!)^{-1}\frac{\partial^m \widehat{f}}{\partial p^m}|_{p=0}, \tag{33}$$

$$\widehat{g} = \sum_{m=1}^{\infty}\widehat{g}_m p^m + \widehat{g}_0, \;\; \widehat{g}_m = (m!)^{-1}\frac{\partial^m \widehat{g}}{\partial p^m}|_{p=0}. \tag{34}$$

It is necessary to choose proper auxiliary parameters for the above series solutions convergence. Thus,

$$\widehat{f} = \sum_{m=1}^{\infty}\widehat{f}_m + \widehat{f}_0, \tag{35}$$

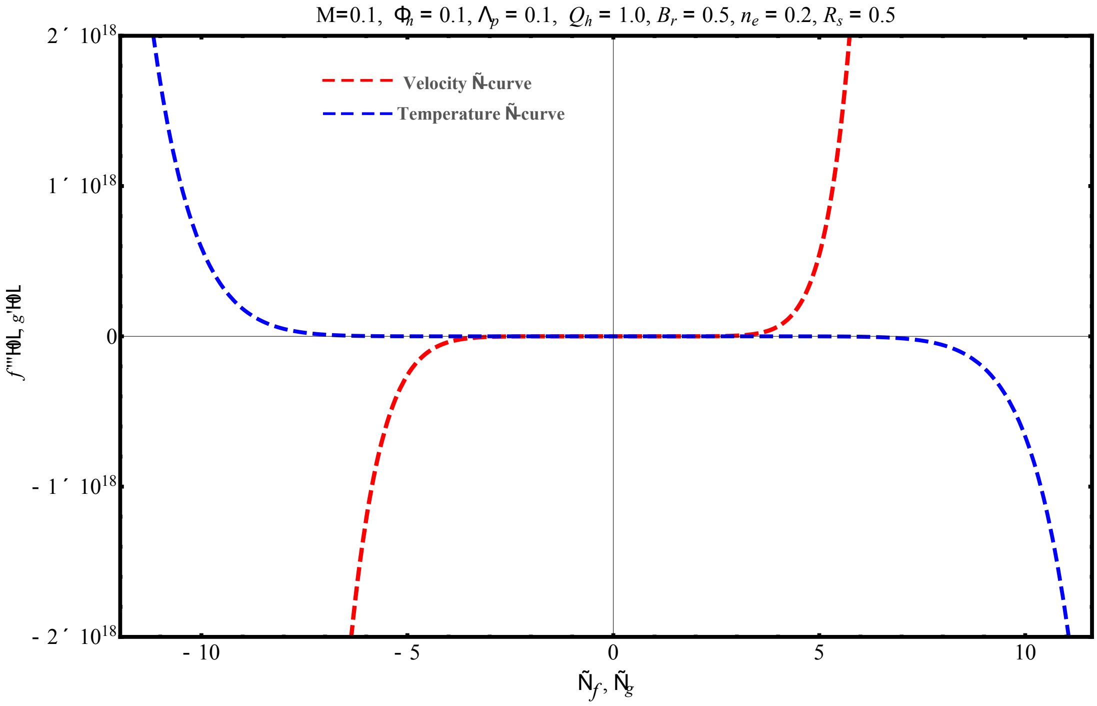

Figure 2: $\hbar$-curves for the $SWCNT_s$ based nanofluid

$$\sum_{m=1}^{\infty} \widehat{g}_m + \widehat{g}_0 = \widehat{g}. \tag{36}$$

The general form of a solutions for the proposed model $(\widehat{f}_m, \widehat{g}_m)$ with the help of a special kind of functions $(\widehat{f}_m^{@}, \widehat{g}_m^{@})$ are

$$\widehat{f}_m = \widehat{f}_m^{@} + M_1 + M_2 exp(\eta) + M_3 exp(-\eta), \tag{37}$$

$$\widehat{g}_m = \widehat{g}_m^{@} + M_4 exp(\eta) + M_5 exp(-\eta). \tag{38}$$

Here, arbitrarily constants are $M_i (i = 1 - 5)$.

3.1. Convergence

The HAM convergence authenticity is based on auxiliary parameters, which are $\hbar_f$ and $\hbar_g$. These parameters work for derived series solution to adjust the convergence. Therefore, Figure 2 and Figure 3 are illustrated to present $\hbar-$ curves for various liquid parameters. A convergence era of $\hbar_f$-curve and $\hbar_g$-curve estimators for $SWCNT_s$ based nanofluid is $-3.5 \leq \hbar_f < 3.5$ and $-6.0 \leq \hbar_g < 7.3$, respectively. Likewise, the convergence of $\hbar_f$-curve and $\hbar_g$-curve estimators for $MWCNT_s$ based nanofluid is $-5.1 \leq \hbar_f < 4.7$ and $-2.0 \leq \hbar_g < 2.0$, respectively.

4. Physical description

The velocity, temperature profiles, and heat transfer rate is committed to analyze in this section by means of involved appropriate boundaries for both types of nanofluid. For this reason, Figures 4-13 are illustrated.

5. Velocity

For a detailed observation of velocity fields $f(\eta)$ against relevant parameters for different CNT_s, Figures 4-8 are developed. Figure 4 illustrates the effect of Marangoni parameter M (flow of a liquid due to gradients in the surface tension of the liquid) on the speed function for both kinds of nanofluids (Water-$SWCNT_s$

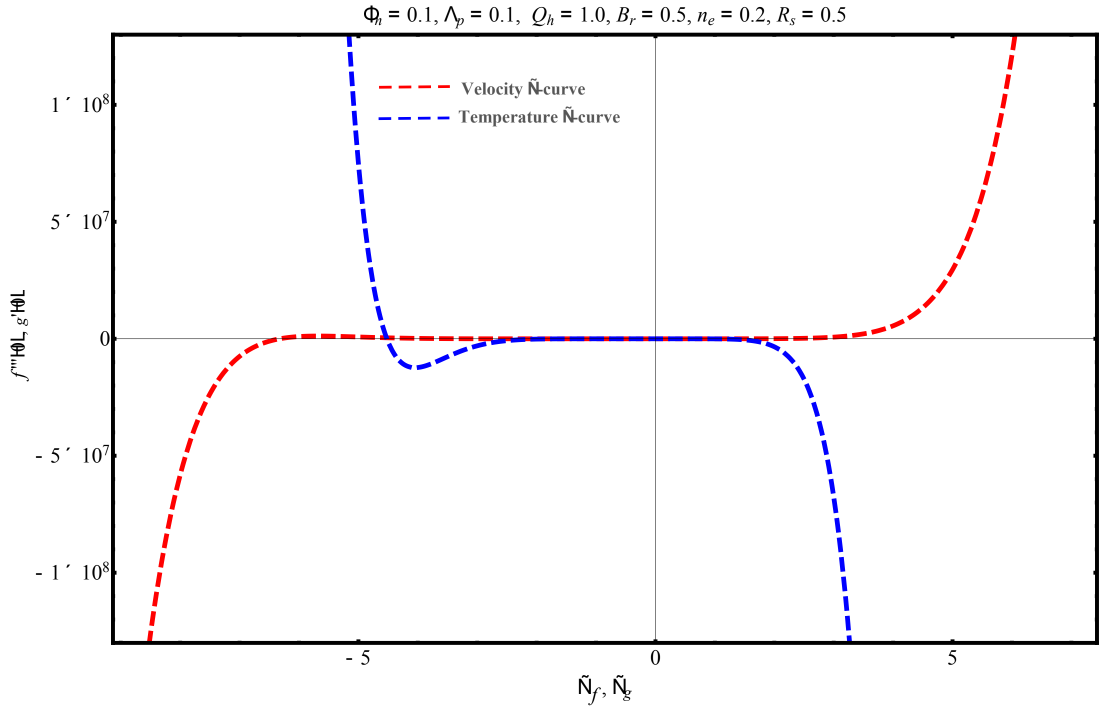

Figure 3: $\hbar$-curves for the $MWCNT_s$ based nanofluid

and Water-$MWCNT_s$). It is noted that motion of fluid speeds up because of higher values of Marangoni parameter for both nanofluids. Physically, this is happening due to high gradients generated in fluid motion which in turns upsurges the fluid motion. In addition, it is seen that Water-$MWCNT_s$ has a better performance than Water-$SWCNT_s$ nanofluids. Figures 5 deals with the impact of nanoparticles solid volume ϕ_n (the ratio among the volume of a constituent and all mixture constituents initial to mixing) against the velocity field for both kinds of nanoparticles. Velocity $f(\eta)$ shows a downward behavior for higher variation in nanoparticle solid volume fraction $\phi_n = 0.01, 0.02, 0.03$. Physically, to develop the dynamical viscosity, strong nano-particles are suspended into the framework. The superb observation has been found for Water-$SWCNT_s$ nanofluid as compared to Water-$MWCNT_s$ nanofluid due to the high density of $SWCNT_s$. Figure 6 demonstrates the features of the velocity profile against the porosity factor λ_p (the volume of pores divided by bulk rock volume). It is noted that magnitude of velocity declines for the larger amount of λ_p for each Water-$SWCNT_s$ and Water-$MWCNT_s$. Physically, this is due to the fact that the outcomes are high dependent to frictional based forces which create deceleration in a fluid velocity. Although in comparison to $SWCNT_s$, the $MWCNT_s$ performs better. Figure 7 shows the trend of velocity against Hartmann value Q_h (the electromagnetic based force divided by viscous force) for both types of nano-structures. Here, $f(\eta)$ rises for larger estimations of Q_h, which is an increasing function of Lorentz forces for both types of nanofluids. Physically, the internal resistance of fluid particles increases due to enlargement in Q_h. One can see that Water-$MWCNT_s$ has an excellent performance with respect to Water-$SWCNT_s$. In Figure 8, the velocity profile is drawn against the exponential index n_e. One can observe a growing behavior of n_e for Water-$SWCNT_s$ as well as for Water-$MWCNT_s$. Aditionally, it is seen that nanoparticle's performance in Water-$SWCNT_s$ is more than as compared to Water-$MWCNT_s$ because $MWCNT_s$ based nanoparticles have more density than $SWCNT_s$. Further, Table 2 presents $-f''(0)$ values for each Water-$SWCNT_s$ and Water-$MWCNT_s$ with respect to different parameters. Water-$SWCNT_s$ nanofluid has a better performance than Water-$MWCNT_s$ due to high density of $SWCNT_s$.

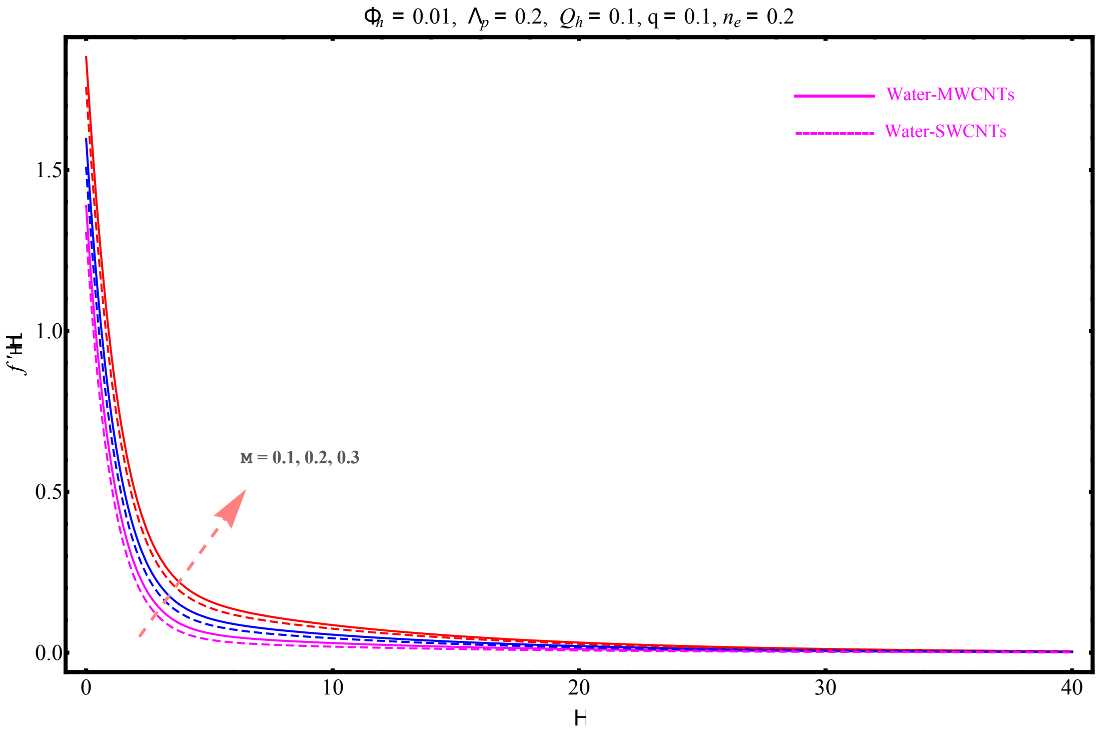

Figure 4: $f'(\eta)$ versus M.

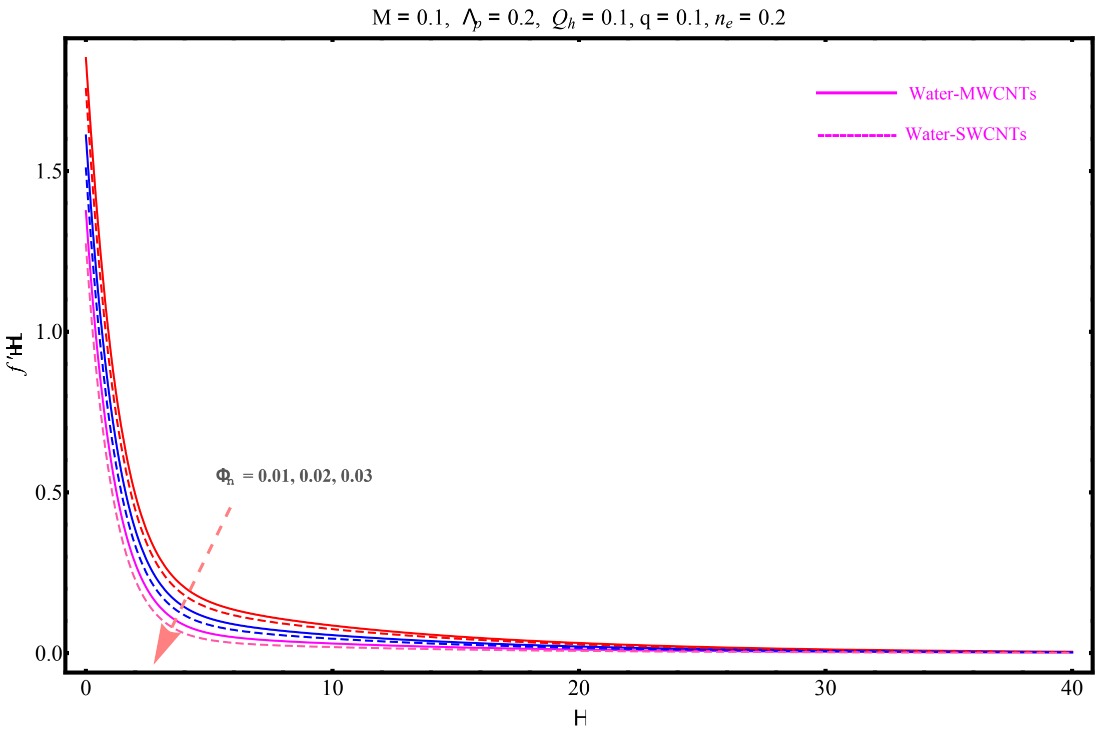

Figure 5: $f'(\eta)$ versus ϕ_n.

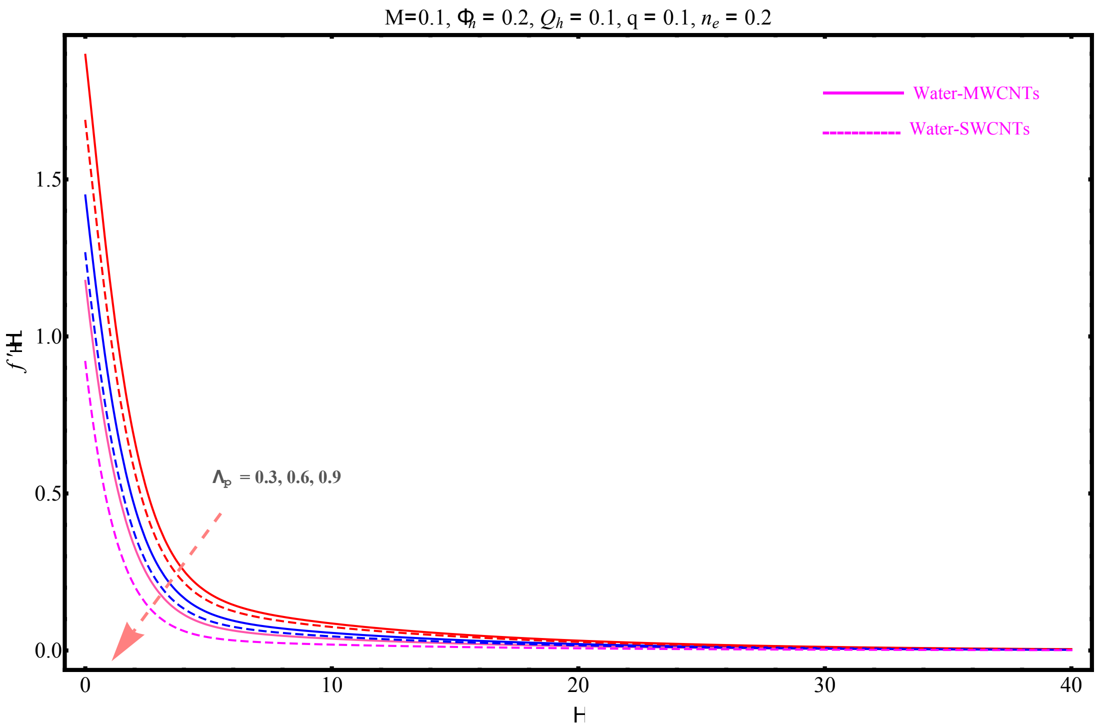

Figure 6: $f'(\eta)$ versus λ_p.

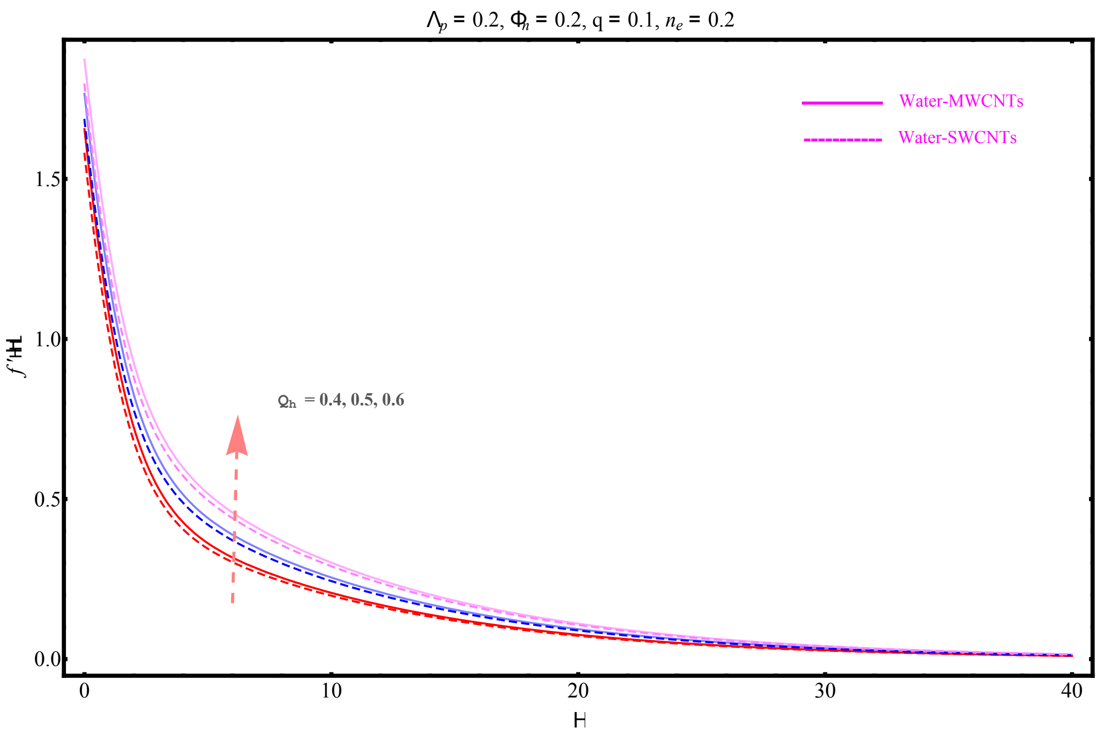

Figure 7: $f'(\eta)$ versus Q_h.

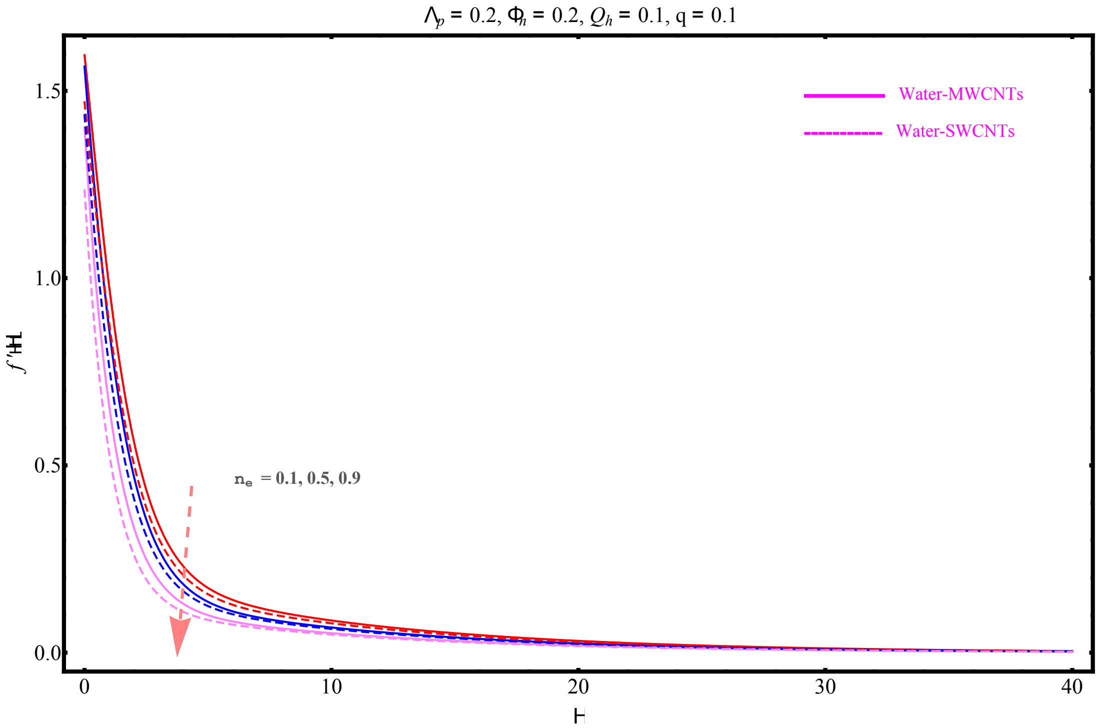

Figure 8: $f'(\eta)$ versus n_e.

Table 2: $-f''(0)$ data for the specified parameters.

n_e	λ_p	Q_h	ϕ_n	M	$SWCNT_s$	$MWCNT_s$
0.1	0.1	0.2	0.1	0.1	0.691949	0.78408
0.3					0.778863	1.00737
0.5					0.98263	0.845264
0.1	0.0	0.2	0.1	0.1	0.856912	0.696652
	0.2				0.694957	0.70241
	0.4				0.700847	0.708013
0.1	0.1	0.0	0.1	0.1	0.845277	0.845277
		0.1			0.618459	0.629774
		0.2			0.691949	0.5746
0.1	0.1	0.2	0.2	0.1	0.661779	0.449839
			0.3		0.517881	0.344886
			0.4		0.400143	0.603713
0.1	0.1	0.2	0.1	0.2	0.355283	0.70241
				0.3	0.697923	0.705231
				0.4	0.700847	0.708013

6. Temperature

Impact of Brinkmann number B_r (the heat generated viscous dissipation divided by molecular conduction based heat transported), radiation parameter R_s (the relative contribution of conduction heat transfer to thermal radiation transfer), nanofluids solid volume fraction ϕ_n (the volume of a constituent divided by the volume of all constituents of the mixture prior to mixing), porosity parameter λ_p (the pores volume divided by the bulk rock volume), and exponential index n_e on temperature profiles for each type of nanofluids can be seen in Figures 9-13. Since, $SWCNT_s$ and $MWCNT_s$ are water based nanofluids therefore, the value of P_r is considered as 6.2. Figure 9 depicts behavior of the temperature profile far away from surface for higher values of B_r. It can be seen that temperature declines for both types of nanofluids. However, the fluid's temperature enhances near to the wall, and there is the intersecting point between fluid temperature line and different CNT_s based nanofluids. For physical point of view, this situation can be clarified as in process of dissipation; thermo-boundary layer suppressed in fluid flow zone by viscosity of fluid and deformative flexibility. Further, Water-$SWCNT_s$ based nanofluid performed well as compared to Water-$MWCNT_s$ nanofluid because $SWCNT_s$ is more conductive than $MWCNT_s$. Figure 10 confirms the variation of $g(\eta)$ against radiation parameter R_s. The temperature declines for higher estimations of R_s whereas temperature increases near the interface and then turn to intersect at $\eta = 1$ for both nanoliquids. Actually,, this has happened due to the wavelength of peak emission in a fluid. Moreover, one can note that Water-$MWCNT_s$ perform excellent than Water-$SWCNT_s$ due to more heat volume of $MWCNT_s$. The significance of the fraction of solid volume for either kinds of nanoparticles on temperature is sketched in Figure 11. The temperature of fluid decays for higher ϕ_n while the initial temperature adopts the upward trend and intersects at $\eta = 1$ for both CNT_s based nanofluids. Physically, an increase in ϕ_n causes an increase in momentum diffusion rate which implies diminishing of the temperature. Further, it is observed that Water-$SWCNT_s$ nanofluid adopted upsurge trend as compared to Water-$MWCNT_s$ nanofluid. Figure 12 delineates the effect of λ_p porosity factor against temperature profile. One can observe that initially, a downward trend in temperature is followed for larger λ_p, soon after for $\eta > 1$, an opposite trend is observed in terms of temperature for either types of nanofluids. Physically, this is attributed to the fact that an increase in permeability means more fluid is allowed to pass far away from surface sheet hence getting heated. This in turn results in enhancement in overall fluid temperature. Finally, Figure 13 depicts the influence of n_e exponential index against temperature for $SWCNT_s$ and $MWCNT_s$ based nanofluids. Results witnessed that the temperature boosts up for higher values of n_e for $\eta > 1$ but near the wall the opposite behavior can be seen and for $\eta = 0.8$ for both nanofluids perform same. This has happened on account of the thickness of thermal boundary layer shoot up for increasing values of exponential index, which enhances the temperature profile. Further, Water-$MWCNT_s$ based nanofluid shows higher than Water-$SWCNT_s$ due to multiple concentric layers of graphene are comprising in the structure of $MWCNT_s$.

6.1. Nusselt number

Table 3 outlines the effects of exponential index n_e, porosity factor λ_p, Hartmann number Q_h, nanoparticle solid volume fraction ϕ_n, radiation parameter R_s, Brinkmann number B_r, and Marangoni convective parameter M, on Nusselt number/rate of heat transfer $Nu_{\widehat{x}}$. Here, one can clearly observe that $Nu_{\widehat{x}}$ is seen high for increased value of n_e, Q_h, ϕ_n, R_s, and M, respectively. However, alternate response is noted in $Nu_{\widehat{x}}$ for higher estimations of λ_p and Brinkmann number B_r. It means that Lorentz forces, radiation, nanoparticle solid volume fraction, and Marangoni parameter are prominent on the heat transfer rate. One can observe that by the variation of ϕ_n, λ_p and R_s, the $MWCNT_s$ based nanoparticles transfer more heat from the fluid rather than the $SWCNT_s$ based nanoparticles. Physically, this is due to high specific heat capacity of $MWCNT_s$ based nanoparticles than $SWCNT_s$ based nanoparticles. Further, $SWCNT_s$ have less surface defect in comparison to $MWCNT_s$ during functionalization. Table 4 is introduced for a parallel comparative analysis and to look over the legitimacy of our solutions. The obtained solutions via HAM have a fantastic agreement with selected parameters for either kinds of nanoliquids; although, the outcomes of GFEM are a bit specific however the version trend is comparable in all of situations.

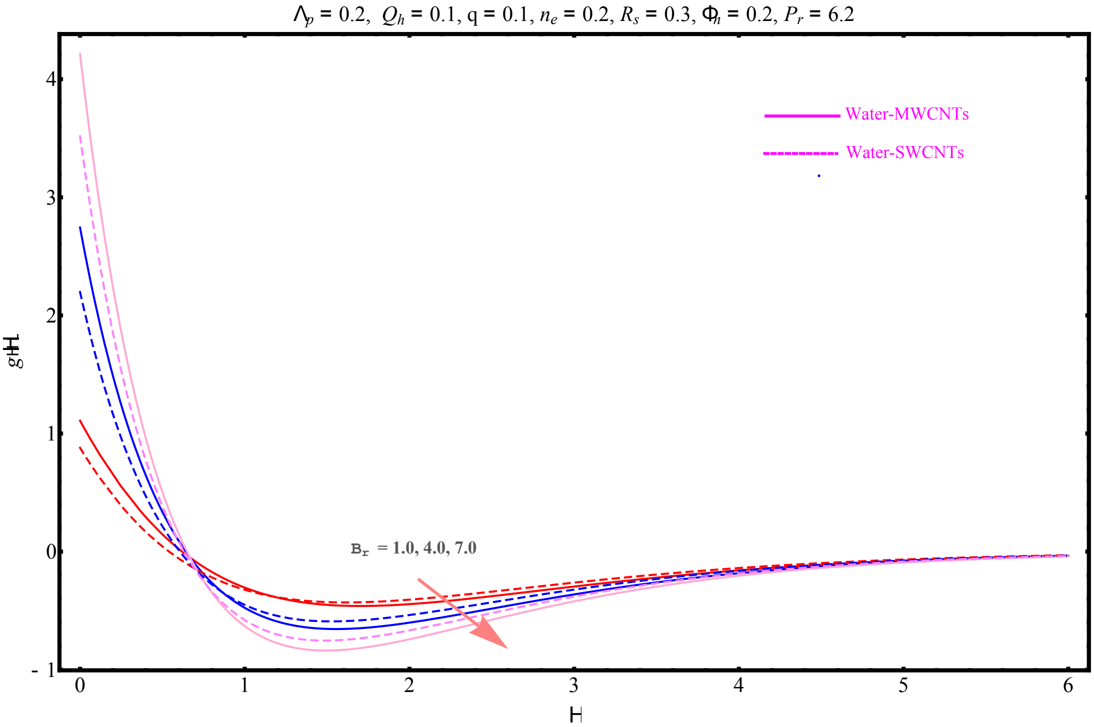

Figure 9: $g(\eta)$ versus B_r.

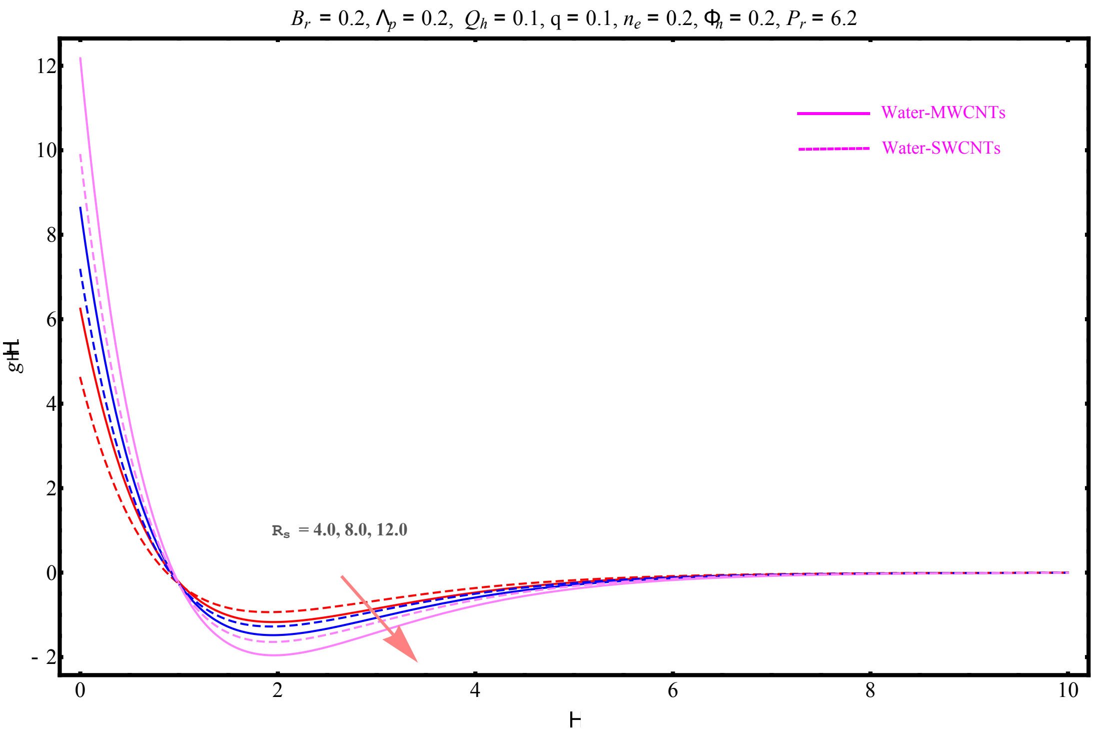

Figure 10: $g(\eta)$ versus R_s.

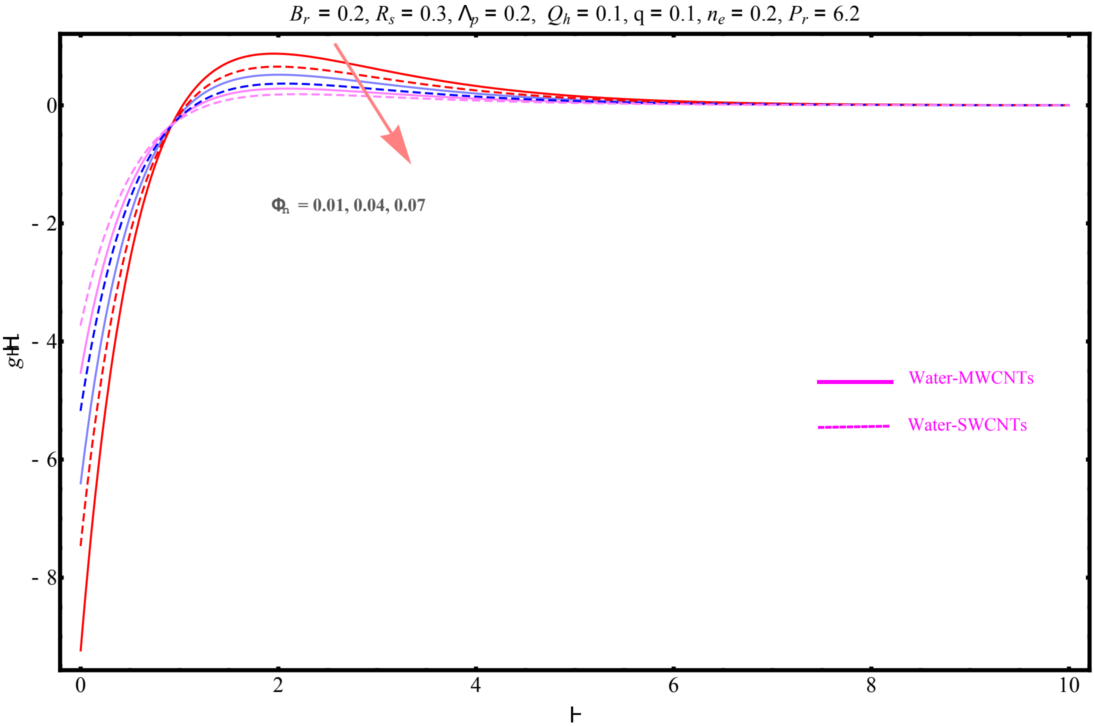

Figure 11: $g(\eta)$ versus ϕ_n.

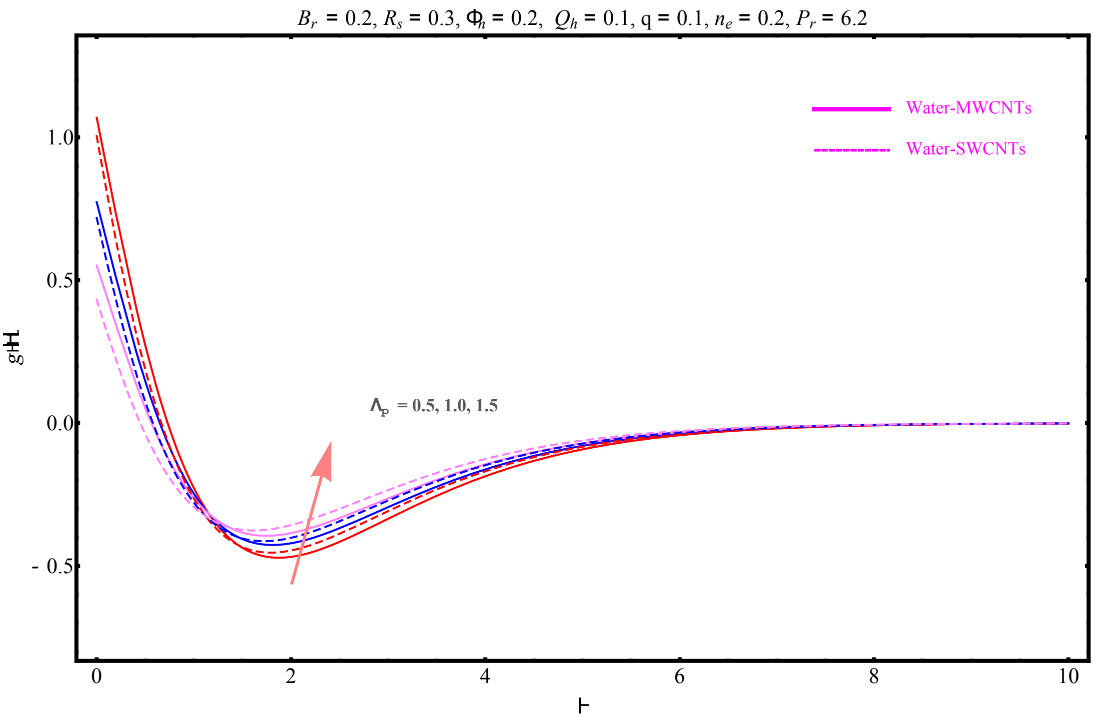

Figure 12: $g(\eta)$ versus λ_p.

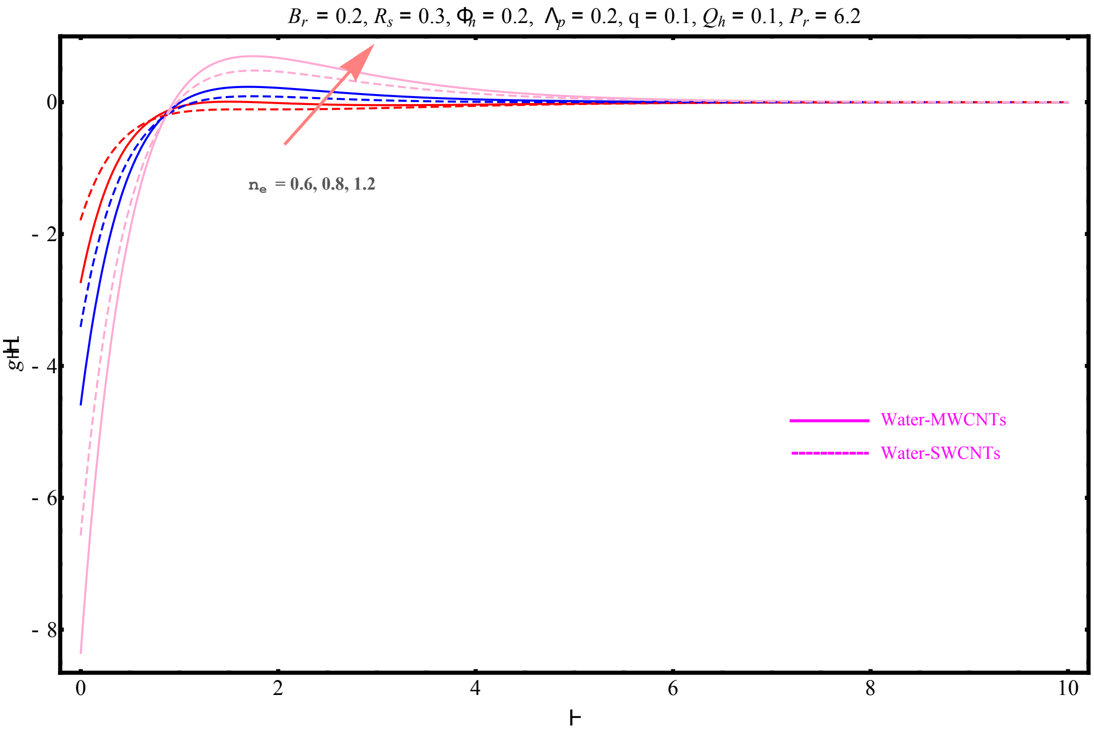

Figure 13: $g(\eta)$ versus n_e.

Table 3: Nusselt number numerical data for the specified parameters.

							$Re_{\widehat{x}}^{\frac{-1}{2}} Nu_{\widehat{x}}$	
n_e	λ_p	Q_h	ϕ_n	R_s	B_r	M	$SWCNT_s$	$MWCNT_s$
0.1	0.1	0.2	0.1	0.2	0.4	0.2	4.4576	3.84545
0.3							4.81999	4.16894
0.5							5.14929	4.4703
0.1	0.0	0.2	0.1	0.2	0.4	0.2	4.57225	3.91481
	0.2						4.35214	3.78034
	0.4						4.16561	3.66203
0.1	0.1	0.0	0.1	0.2	0.4	0.2	3.80422	3.4942
		0.1					4.13296	3.67012
		0.2					4.4576	3.84545
0.1	0.1	0.2	0.2	0.2	0.4	0.2	6.31326	5.4951
			0.3				7.71553	6.79265
			0.4				8.74407	7.73593
0.1	0.1	0.2	0.1	0.3	0.4	0.2	4.57038	3.95305
				0.5			4.79127	4.16424
				0.7			5.5467	4.37022
0.1	0.1	0.2	0.1	0.2	0.2	0.2	4.0694	3.87436
					0.6		4.00917	3.81654
					0.8		3.97905	3.78763
0.1	0.1	0.2	0.1	0.2	0.4	0.1	6.12326	5.9451
						0.3	7.17553	6.97265
						0.5	8.47407	7.37593

Table 4: Comparative data of $-g'(0)$ with GFEM [40].

n_e	ϕ_n	λ_p	Q_h	R_s	B_r	M	$SWCNT_s$		$MWCNT_s$	
							GFEM	**HAM**	**GFEM**	**HAM**
0.1	0.1	0.2	0.1	0.50	0.1	0.0	1.4334266	1.40118	1.5338833	1.59703
	0.04						1.9510110	1.8684	2.0119659	2.34384
	0.1	0.4					-	1.81845	-	1.52405
		0.2	0.1			0.0	1.4334266	1.40118	1.5338833	1.59703
				3.0			1.2928663	1.24689	1.379143	1.30881
				0.50	1.0		1.3230864	1.36729	1.4214820	1.41694

7. Concluding remarks

The effects of Lorentz forces, porosity factor, viscous dissipation, thermal radiation, and Marangoni convection in nanoliquid with different types of CNT_s based nanoparticle aggregation such as Water-$SWCNT_s$ and Water-$MWCNT_s$ are investigated in this research. The governing equations are coupled due to the presence of Marangoni (thermocapillary) convection. The observation indicated that the profile of velocity seems to be an upward trend via Hartmann number Q_h and Marangoni parameter M for both $SWCNT_s$ and $MWCNT_s$ based nanoliquid in fluid flow. The velocity profile shows decline behavior for the larger amounts of n_e, λ_p, and ϕ_n for $SWCNT_s$ and $MWCNT_s$ based nanofluid. The presence of Q_h, ϕ_n, R_s, and B_r show decrease in the temperature profile for either kinds of nanoparticles. The temperature profile boosts up for growing amount of porosity term λ_p and exponent term n_e for each kind of nanofluids. Further, the rate of heat transfer speeds up for Hartmann number Q_h, fraction of solid volume of nanoparticles ϕ_n, Radiation R_s, exponential term n_e, and Marangoni parameter M while the opposite trend is for Brinkman number B_r and observe porosity factor λ_p for $SWCNT_s$ as well as for $MWCNT_s$ nanoparticles.

References

[1] L. Liu, L. Feng, Q. Xu, L. Zheng and F. Liu, Flow and heat transfer of generalized Maxwell fluid over a moving plate with distributed order time fractional constitutive models, Int. Commun. Heat Mass Transf., 116 (2020) 104-679.

[2] S. Yang, L. Liu, Z. Long and L. Feng, Unsteady natural convection boundary layer flow and heat transfer past a vertical flat plate with novel constitution models, Appl. Math. Lett., 120 (2021) 107-335.

[3] S.U. Choi and J.A. Eastman, Enhancing thermal conductivity of fluids with nanoparticles, Argonne National Lab, (1995).

[4] B. Mahanthesh, Flow and heat transport of nanomaterial with quadratic radiative heat flux and aggregation kinematics of nanoparticles, Int. Commun. Heat Mass Transf., 127 (2021) 105-521.

[5] P. Rana, B. Mahanthesh, J. Mackolil and W. Al-Kouz, Nanofluid flow past a vertical plate with nanoparticle aggregation kinematics, thermal slip and significant buoyancy force effects using modified Buongiorno model, Waves in Random and Complex Media, (2021) 1-25.

[6] K. Swain and B. Mahanthesh, Thermal enhancement of radiating magneto-nanoliquid with nanoparticles aggregation and joule heating: a three-dimensional flow, Arab J. Sci. Eng., 46(6) (2021) 5865-5873.

[7] B. Mahanthesh, B.J. Gireesha, R. Gorla, F.M. Abbasi and S.A. Shehzad, Numerical solutions for magnetohydrodynamic flow of nanofluid over a bidirectional non-linear stretching surface with prescribed surface heat flux boundary, J. Magn. Magn., 417 (2016) 189-196.

[8] A.S. Sabu, J. Mackolil, B. Mahanthesh and A. Mathew, Nanoparticle aggregation kinematics on the quadratic convective magnetohydrodynamic flow of nanomaterial past an inclined flat plate with sensitivity analysis, P I MECH. ENG. E-J PRO., (2021).

[9] F. Ahmed, M.A. Abir, M. Fuad, F. Akter, P.K. Bhowmik, S.B. Alam and D. Kumar, Numerical investigation of the thermo-hydraulic performance of water-based nanofluids in a dimpled channel flow using Al2O3, CuO, and hybrid Al2O3 CuO as nanoparticles, J. Heat Transfer, 50(5) (2021) 5080-5105.

[10] P.S. Reddy and P. Sreedevi, Effect of thermal radiation and volume fraction on carbon nanotubes based nanofluid flow inside a square chamber, Alex. Eng. J., 60(1) (2021) 1807-1817.

[11] Z. Ahmed, S. Saleem, S. Nadeem and A.U. Khan, Squeezing flow of Carbon nanotubes-based nanofluid in channel considering temperature-dependent viscosity: a numerical approach, *Arab. J. Sci. Eng.*, 46(3) (2021) 2047-2053.

[12] T. Gul, M. Bilal, W. Alghamdi, M.I. Asjad and T. Abdeljawad, Hybrid nanofluid flow within the conical gap between the cone and the surface of a rotating disk, Sci. Rep., 11(1) (2021) 1-19.

[13] I. Zari, A. Shafiq, T.S. Khan and S. Haq, Marangoni Convective Flow of GO-kerosene-and GO-water-based Casson Nanoliquid Toward a Penetrable Riga Surface, Braz. J. Phys., (2021) 1-16.

[14] T. Gul, B. Ali, W. Alghamdi, S. Nasir, A. Saeed, P. Kumam and M. Jawad, Mixed convection stagnation point flow of the blood based hybrid nanofluid around a rotating sphere, Sci. Rep., 11(1) (2021) 1-15.

[15] M.I. Khan, Transportation of hybrid nanoparticles in forced convective Darcy-Forchheimer flow by a rotating disk, *Int. Commun. Heat Mass Transf.*, 122 (2021) 105-177.

[16] D.R.V.S.R.K. Sastry, A.S.N. Murti and T.P. Kantha, The effect of heat transfer on MHD Marangoni boundary layer flow past a flat plate in nanofluid, Int. J. Eng. Math., (2013).

[17] D.R.V.S.R.K. Sastry, Thermosolutal MHD marangoni convective flow of a nanofluid past a flat plate with viscous dissipation and radiation effects, WSEAS Trans. Math., 15 (2016) 271-279.

[18] D.R.V.S.R.K. Sastry, P.K. Kameswaran, P. Sibanda and P. Sudhagar, Soret and Dufour Effects on Hydromagnetic Marangoni Convection Boundary Layer Nanofluid Flow Past a Flat Plate, Appl. Math. Comput., (2019) 439-449.

[19] D.R.V.S.R.K. Sastry and P.K. Kameswaran, MHD and Viscous Dissipation Effects in Marangoni Mixed Flow of a Nanofluid over an Inclined Plate in the Presence of Ohmic Heating, Fluid Dyn. Mater. Proce., 17 (2021).

[20] T. Gul, M.Z. Ullah, A.K. Alzahrani, Z. Zaheer and I.S. Amiri, MHD thin film flow of kerosene oil based CNTs nanofluid under the Influence of Marangoni convection, Phys. Scr., 95(1) (2020) 15-702.

[21] Y. Zhang, Y. Zhang, Y. Bai, B. Yuan and L. Zheng, Flow and heat transfer analysis of a maxwell-power-law fluid film with forced thermal Marangoni convective, Int. Commun. Heat Mass Transf., 121 (2021) 105-162.

[22] T. Gul, H. Anwar, M.A. Khan, I. Khan and P. Kumam, Integer and non-integer order study of the GO-W/GO-EG nanofluids flow by means of Marangoni convection, Symmetry, 11(5) (2019) 640.

[23] S. Qayyum, Dynamics of Marangoni convection in hybrid nanofluid flow submerged in ethylene glycol and water base fluids, Int. Commun. Heat Mass Transf., 119 (2020) 104-962.

[24] A. Gailitis, On the possibility to reduce the hydrodynamic drag of a plate in an electrolyte, Rep. Inst. Phys. Riga 13 (1961) 143-146.

[25] H. Vaidya, K.V. Prasad, I. Tlili, O.D. Makinde, C. Rajashekhar, S.U. Khan and D.L. Mahendra, Mixed convective nanofluid flow over a non linearly stretched Riga plate, Case Stud. Therm. Eng., 24 (2021) 100-828.

[26] N.S. Khashi'ie, N.M. Arifin, I. Pop and N.S. Wahid, Effect of suction on the stagnation point flow of hybrid nanofluid toward a permeable and vertical Riga plate, Heat Trans., 50(2) (2021) 1895-1910.

[27] M. Nazeer, M.I. Khan, M.U. Rafiq and N.B. Khan, Numerical and scale analysis of Eyring-Powell nanofluid towards a magnetized stretched Riga surface with entropy generation and internal resistance, I. Commun. Heat and Mass Trans., 119 (2020) 104-968.

[28] M.M. Bhatti and E.E. Michaelides, Study of Arrhenius activation energy on the thermo-bioconvection nanofluid flow over a Riga plate, J. Therm. Anal. Calorim. 143(3) (2021) 2029-2038.

[29] Z. Iqbal, E. Azhar, Z. Mehmood and E.N. Maraj, Melting heat transport of nanofluidic problem over a Riga plate with erratic thickness: use of Keller Box scheme, Results Phys. 7 (2017) 3648-3658.

[30] S. Nadeem, N. Abbas and M.Y. Malik, Heat transport in CNTs based nanomaterial flow of non-Newtonian fluid having electro magnetize plate, Alex. Eng. J., 59(5) (2020) 3431-3442.

[31] F.O.M. Mallawi, M. Bhuvaneswari, S. Sivasankaran and S. Eswaramoorthi, Impact of double-stratification on convective flow of a non-Newtonian liquid in a Riga plate with Cattaneo-Christov double-flux and thermal radiation, Ain Shams Eng. J., 12(1) (2021) 969-981.

[32] B. Ali, P.K. Pattnaik, R.A. Naqvi, H. Waqas and S. Hussain, Brownian motion and thermophoresis effects on bioconvection of rotating Maxwell nanofluid over a Riga plate with Arrhenius activation energy and Cattaneo-Christov heat flux theory, Therm. Sci. Eng. Prog., 23 (2021) 100-863.

[33] J.K. Madhukesh, G.K. Ramesh, E.H. Aly and A.J. Chamkha, Dynamics of water conveying SWCNT nanoparticles and swimming microorganisms over a Riga plate subject to heat source/sink, Alex. Eng. J., (2021).

[34] L. Noeiaghdam, S. Noeiaghdam and D. Sidorov, Dynamical control on the homotopy analysis method for solving nonlinear shallow water wave equation, J. Phys., 1847(1) (2021) 100-112.

[35] B.M. Yambiyo, F. Norouzi and G.M. Guerekata, A study of an epidemic SIR model via Homotopy Analysis Method in the sense of Caputo-fractional system, Stud. Evol. Eqs. STEAM-H series, (2021).

[36] H. Chen and Y. Wang, Homotopy Analysis Method for a Conservative Nonlinear Oscillator with Fractional Power, J. Appl. Math. Phys., 9(1) (2021) 31.

[37] C.L. Ejikeme, M.O. Oyesanya, D.F. Agbebaku and M.B. Okofu, Discussing a Solution to Nonlinear Duffing Oscillator with Fractional Derivatives Using Homotopy Analysis Method (HAM), T. Prac. Math. Comp. Sci., 6 (2021) 57-81.

[38] Z. Odibat and A. Sami Bataineh, An adaptation of homotopy analysis method for reliable treatment of strongly nonlinear problems: construction of homotopy polynomials, Mathemat. Methods Appl. Sci., 38(5) (2015) 991-1000.

[39] K. Hosseini, K. Sadri, M. Mirzazadeh, A. Ahmadian, Y.M. Chu and S. Salahshour, Reliable methods to look for analytical and numerical solutions of a nonlinear differential equation arising in heat transfer with the conformable derivative, Mathemat. Methods Appl. Sci., (2021).

[40] S. Chaudhary and K.M. Kanika, Radiation heat transfer on SWCNT and MWCNT based magnetohydrodynamic nanofluid flow with marangoni convection, Physica Scripta 95(2) (2019).

[41] I. Zari, A. Shafiq and T.S. Khan, Simulation study of Marangoni convective flow of kerosene oil based nanofluid driven by a porous surface with suction and injection, I. Communs. Heat and Mass Trans., 127 (2021) 105-493.

[42] I. Zari, A. Shafiq, G. Rasool, T.N. Sindhu and T.S. Khan, Double-stratified Marangoni boundary layer flow of Casson nanoliquid: probable error application, J. Thermal Analy. Calorimetry, 147(12) (2022) 6913-6929.

[43] A. Shafiq, I. Zari, I. Khan, T.S. Khan, A.H. Seikh and E.S.M. Sherif, Marangoni driven boundary layer flow of carbon nanotubes toward a Riga plate, Front. Phys., 7 (2020) 215.

[44] C.L. Ejikeme, M.O. Oyesanya, D.F. Agbebaku and M.B. Okofu, Discussing a Solution to Nonlinear Duffing Oscillator with Fractional Derivatives Using Homotopy Analysis Method (HAM), T. P. Math. Comp. Sci., 6 (2021) 57-81.

[45] H. Singh, Analysis of drug treatment of the fractional HIV infection model of CD4+ T-cells, Chaos, Sols. Fra., 146 (2021) 110-868.

[46] L. Noeiaghdam, S. Noeiaghdam and D. Sidorov, Dynamical control on the homotopy analysis method for solving nonlinear shallow water wave equation, I.J.Phys., 1847(1) (2021).

[47] Y. Chen, S. Dong, Z. Zang, C. Ao, H. Liu, M. Gao and J. Cao, Buckling analysis of subsea pipeline with idealized corrosion defects using homotopy analysis method, Ocean Eng., (2021) 108-865.

[48] Z. Zhunussova, Nonlinear PDE as immersions, Trends in Mathematics, 2 (2015) 289–297.

[49] A.F.A. Elbarghthi, H.M. Yousef, D. Václav; Heat Transfer Analysis between R744 and HFOs inside Plate Heat Exchangers Entropy 24(8) (2022) 11-50.

[50] R.I. Khrapko, Lorentz force in the absence of charges and currents. J. Modern. Opt. 69(18) (2022) 1060–1061.

[51] U. Khan, A. Zaib, A. Ishak, S.A. Bakar, M. Taseer Numerical simulations of bio-convection in the stream-wise and cross-flow directions comprising nanofluid conveying motile microorganism: analysis of multiple solutions. Int. J. Comput. Methods 19(1) (2022) 32.